2011 American Control Conference
on O'Farrell Street, San Francisco, CA, USA
June 29 - July 01, 2011

Adaptive Control of a Solid Oxide Fuel Cell Ultra-Capacitor Hybrid System

Tuhin Das and Steven Snyder

Abstract— **Solid oxide fuel cells (SOFCs) offer a number of advantages beyond those of most other fuel cells. However, like other fuel cells, rapid load following is difficult, and can lead to fuel starvation and consequently fuel cell damage. Mitigating fuel starvation and improving load following capabilities are conflicting control objectives. However, the issue can be addressed by the hybridization of the system with an energy storage device. A steady-state utilization property, combined with a current regulation strategy, is used to manage transient fuel utilization. Meanwhile, an overall system strategy is employed to manage energy sharing in the hybrid system for load following as well as for maintaining the state-of-charge of the energy storage device. This work presents an adaptive strategy which updates the controller based on current parameter estimates. The control design is validated on a hardware-in-the-loop setup and experimental results are provided.**

I. INTRODUCTION

The Solid Oxide Fuel Cell (SOFC) has shown significant potential as an efficient energy conversion device. SOFCs operate at high temperatures (800 – 1000 °C). This gives SOFCs advantages beyond those shared with most other fuel cells, such as tolerance to impurities and internal reforming (and consequently a larger fuel flexibility), heat as a byproduct (useful for co-generation or in a bottoming cycle), and faster reaction kinetics without precious metal (platinum) catalysts [1], [2], [3].

Despite the efficiency and versatility of SOFCs, there are some limitations. One disadvantage common to all fuel cells is their lack of dynamic load following capabilities [4]. This is generally attributed to the fuel delivery system of SOFCs and its slower mechanical subsystems, such as pumps, valves and reformers, [5], [6], [7], [8]. When exposed to large power fluctuations, hydrogen starvation can occur due to the slower fuel supply, potentially resulting in voltage drop, anode oxidation, and catalyst corrosion [8], [9], which are detrimental to cell integrity and efficiency.

To monitor hydrogen starvation, the system performance is often characterized by the parameter U, or fuel utilization. Fuel utilization is defined as the ratio of hydrogen consumption to the net available hydrogen in the anode [10]. In order to balance fuel efficiency and safe operation, target U values typically range between 80% and 90% [10], [11], [12]. Power fluctuations cause transience in the utilization. Therefore, maintaining the target U and mitigating the effects of power fluctuations are important in any SOFC system.

This work was supported by the Office of Naval Research under grant #N000140910272.

T. Das is an Assistant Professor and S. Snyder is a graduate student of Mechanical Engineering at Rochester Institute of Technology, Rochester, NY 14623, USA, tkdeme@rit.edu

In this paper, we address the issue of fuel starvation through transient control of U using a current regulation mechanism that uses a steady-state invariant relationship relating U, current draw and fuel supply rate. This method was developed in our prior research, [13], [14]. Existing approaches for preventing oxygen starvation in PEM fuel cells using filtering, Model Predictive Control (MPC) and robust load governor designs, appear in [15], [16], [7], [17]. To improve load following, we hybridize the fuel cell with an ultra-capacitor interfaced through DC/DC converters. There is considerable existing work in the literature on control of hybrid fuel cell ultra-capacitor/battery systems, such as the references above as well as [18], [19], [20], [21]. A majority of the existing work consider PEM (Polymer Electrolyte Membrane) fuel cells. The novelty of the work presented in this paper lies in the adaptive control formulation for the hybridized SOFC system. The formulation incorporates current regulation and the controller simultaneously maintains the state-of-charge of the ultra-capacitor at a target level. In the proposed adaptive strategy, the unknown and varying efficiencies of the DC/DC converters are estimated through adaptation laws in suitable parametric form.

This paper is organized as follows. In section II, we describe the SOFC system under consideration and briefly outline the current regulation strategy. In section III, we propose the adaptive control design and provide a stability analysis. Experimental results of control validation using our existing hardware-in-the-loop test-system is provided in section 5. Concluding remarks are provided in section V, followed by references.

II. BACKGROUND

A. SYSTEM OVERVIEW

The specific system considered in this paper is a steam reformer based SOFC system with methane as fuel, shown schematically in Fig.1. However, the control approach presented in this paper can be extended to other fuels and system configurations. The reformer produces a hydrogen-rich gas which is supplied to the anode of the fuel cell. Electrochemical reactions occurring at the anode due to current draw results in a steam-rich gas mixture at its exit. A known fraction k of the anode exhaust is recirculated through the reformer into a mixing chamber where fuel $\dot{N}_f$ is added. Fuel is supplied by the fuel supply system (FSS). The FSS consists of a fuel pump and/or valves and a fuel flow controller. The heat required for sustaining the endothermic steam reforming process occurring in the reformer catalyst bed is supplied from two sources, namely, the

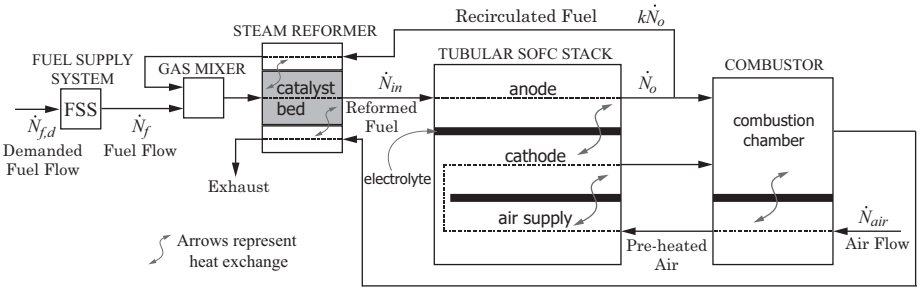

Fig. 1. Schematic of SOFC System

combustor exhaust that is passed through the reformer, and the aforementioned recirculated anode flow. The combustor also serves to preheat the cathode air $\dot{N}_{air}$. The tubular construction of each cell causes the air to first enter the cell through the air supply tube and then reverse its direction to enter the cathode chamber. For steam reforming of methane we consider a packed-bed tubular reformer with nickel-alumina catalyst. We use a control-oriented mathematical model of a tubular SOFC system developed in our prior research, presented in [22], for control validation. The model captures the thermodynamics, chemical kinetics, heat transfer and pressure dynamics phenomena and has been validated against results in literature.

As mentioned in the Introduction, load following is achieved through hybridization of the fuel cell with an ultra-capacitor. A schematic diagram showing the hybridization and the control interface is shown in Fig. 2. The fuel cell and ultra-capacitor are connected in parallel. The fuel cell supplies power to the load through a uni-directional DC/DC converter C_1. The ultra-capacitor is connected to the load through a bi-directional DC/DC converter C_2 allowing charge and discharge. Based on the hybrid system schematic in Figure 2, the instantaneous power balance equation is

$$V_L i_L = \eta_1 V_{fc} i_{fc} + \eta_2 V_{uc} i_{uc} \tag{1}$$

Certain salient aspects of the hybrid interface and control design are given below:

1) The bus voltage (V_L) is held constant. This is possible by operating either C_1 or C_2 in voltage control mode while the other operates in current control mode. Without loss of generality, C_1 will be in voltage control mode, while C_2 follows the commanded ultra-capacitor current.
2) The ultra-capacitor current, i_{uc}, and the fuel demand, $\dot{N}_{f,d}$, are treated as control inputs.
3) V_{fc}, V_{uc}, i_L, i_{fc}, and $\dot{N}_f$ are measured.
4) The DC/DC converter efficiencies, η_1 and η_2, are unknown and variable with known upper and lower bounds. The variations in efficiencies are assumed to be slowly varying parameters. Controller estimates for the efficiencies are denoted as $\bar{\eta}_1$ and $\bar{\eta}_2$.

B. CURRENT REGULATION

In prior work, a feedback based strategy for minimizing fluctuations in fuel utilization was presented. This method, described briefly below, is used within the hybrid system to

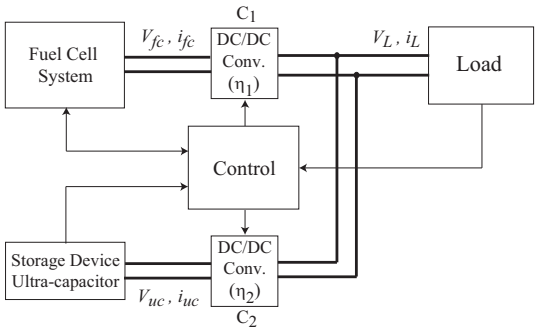

Fig. 2. Schematic of Hybrid Fuel Cell System

control the fuel cell. For further description and explanation of this strategy, please refer to [13].

Based on the molar balance equations and the rate of electrochemical reaction, a steady state relationship of the utilization can be described as in Eq.(2) below, where k is a known fraction of the anode exhaust flow that is recirculated, $\mathcal{N}_{cell}$ is the number of cells in series, $n = 2$ is the number of electrons produced in the electrochemical reaction, $F = 96485.34$Coul./mol is Faraday's constant, $\dot{N}_f$ is the measured fuel flow, and i_{fc} is the fuel cell current.

$$U_{ss} = \frac{1-k}{(4nF\dot{N}_f/i_{fc}\mathcal{N}_{cell}) - k} \tag{2}$$

Notice that all of these quantities are measurable or known and Eq.(2) is invariant with respect to reformer reaction rates, internal reaction rates, temperatures, pressures and internal flow rates. Thus, Eq.(2) can be said to be an invariant relationship of the fuel cell. For a target U_{ss} and a demanded fuel cell current $i_{fc,d}$, a fuel flow demand, $\dot{N}_{f,d}$, can be calculated from this relationship as in Eq.(3).

$$\dot{N}_{f,d} = \frac{i_{fc,d}\mathcal{N}_{cell}}{4nFU_{ss}}[1-(1-U_{ss})k] \tag{3}$$

However, during transience, due to the lag associated with the fuel supply system (FSS, Fig.1), the actual fuel flow is not equal to the demanded fuel flow. This results in fluctuations in the utilization. For large changes in the current demand, this can result in hydrogen starvation. To address this, Eq.(3) can be reversed in order to regulate current based on the actual fuel flow, given below

$$i_{fc} = \frac{4nFU_{ss}\dot{N}_f}{\mathcal{N}_{cell}} \frac{1}{[1-(1-U_{ss})k]} \tag{4}$$

This current regulation approach is illustrated in Fig.3. It is a simple yet effective means for considerably attenuating

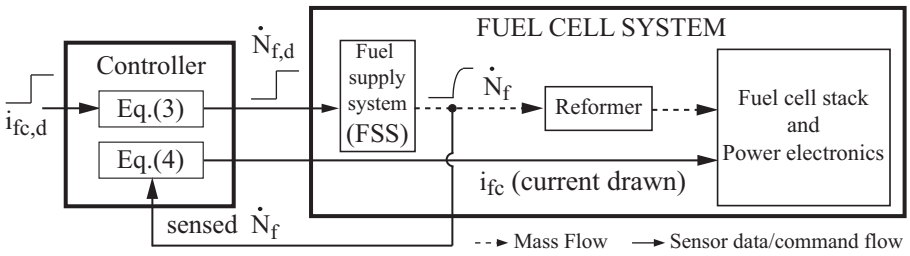

Fig. 3. Transient Control of U through Current Regulation

transient fluctuations in U even for significant fluctuations in power demand and assumes no knowledge of the dynamic characteristics of the FSS, [13].

However, this strategy also creates a disparity between the demanded fuel cell current, $i_{fc,d}$, and the actual delivered current, i_{fc} during transients. This disparity is addressed by hybridizing the fuel cell with an ultra-capacitor. Adding the ultra-capacitor requires that its state-of-charge (SOC) is maintained in order to avoid charge depletion or overcharge.

III. CONTROL DEVELOPMENT

A. ADAPTIVE CONTROLLER

A schematic representation of the adaptive controller is depicted in Fig. 4. Details of the control design will be presented in this section. As mentioned in section II-A, i_{uc} and $\dot{N}_{f,d}$ are the control inputs. The control objectives are, to maintain the SOC of the ultra-capacitor at a target value (80% in this case) and to incorporate the fuel cell current regulation approach of section II-B, while treating the DC/DC converter efficiencies η_1, η_2 as unknown and slowly varying parameters. The adaptive controller will be designed to estimate these efficiencies. Other considerations for control are listed in section II-A.

We design the fuel cell to serve as the primary energy source with the ultra-capacitor simply supplying transient demand. Hence the instantaneous fuel cell current demand is governed by Eq.(5) in the presence of uncertainties. The state of charge, denoted S, is calculated as the ratio of the ultra-capacitor voltage, V_{uc}, to its maximum voltage, V_{max}. The target steady-state value of S is denoted as S_t.

$$i_{fc,d} = \frac{V_L i_L}{\bar{\eta}_1 V_{fc}} - k_s E_s,\ E_s = S - S_t,\ S = \frac{V_{uc}}{V_{max}},\ k_s > 0 \tag{5}$$

In Eq.(5), k_s is a constant to be chosen appropriately. The actual control input, $\dot{N}_{f,d}$, is an algebraic function of $i_{fc,d}$ that satisfies the desired U_{ss}, Eq.(3). The ultra-capacitor current command is calculated by Eq.(6). Here the function $h(E_{fc})$ is designed to attain the target fuel cell current $i_{fc,t}$ (calculated using Eq.(4)) and consequently, achieve the target steady-state utilization U_{ss}. The term $h(E_{fc})$ takes the form of a PD controller for this work.

$$\begin{aligned} i_{uc} = i_{uc,c} &= V_L i_L - \bar{\eta}_1 V_{fc} i_{fc,t}/(\bar{\eta}_2 V_{uc}) + h(E_{fc}), \\ E_{fc} &= i_{fc} - i_{fc,t}, \\ h(E_{fc}) &= k_p E_{fc} + k_d \dot{E}_{fc},\ k_p, k_d > 0 \end{aligned} \tag{6}$$

Note that the designs of $i_{fc,d}$ and i_{uc} involve estimates of the DC/DC converter efficiencies $\bar{\eta}_1$ and $\bar{\eta}_2$. We propose the following parametric forms of the efficiencies:

$$\beta_1 = \frac{1}{\eta_1},\quad \beta_2 = \frac{1}{\eta_2},\quad \beta_{12} = \frac{\eta_1}{\eta_2} \tag{7}$$

with

$$\bar{\beta}_1 = \frac{1}{\bar{\eta}_1},\quad \bar{\beta}_2 = \frac{1}{\bar{\eta}_2},\quad \bar{\beta}_{12} = \frac{\bar{\eta}_1}{\bar{\eta}_2} \tag{8}$$

representing the parameter estimates and

$$e_1 = \beta_1 - \bar{\beta}_1,\quad e_2 = \beta_2 - \bar{\beta}_2,\quad e_{12} = \beta_{12} - \bar{\beta}_{12} \tag{9}$$

representing the parameter errors. We next propose the following parameter adaptation laws:

$$\begin{aligned} \dot{\bar{\beta}}_1 &= -\tfrac{V_L i_L E_s}{C V_{max} V_{uc}}\gamma_1 + g_1, \quad \dot{\bar{\beta}}_2 = \tfrac{V_L i_L E_{fc}}{V_{uc}}\gamma_2 + g_2 \\ \dot{\bar{\beta}}_{12} &= -\tfrac{V_{fc} i_{fc} E_{fc}}{V_{uc}}\gamma_{12} + g_{12}, \quad 0 < \gamma_1, \gamma_2, \gamma_{12} \end{aligned} \tag{10}$$

where, γ_1, γ_2 and γ_{12} are constant parameter adaptation gains. The terms g_1, g_2 and g_{12} are designed as follows, to maintain boundedness of parameter estimates:

$$\begin{aligned} g_1 &= \begin{cases} -d_1 & \text{if } \bar{\beta}_1 \geq \beta_{1,max} \text{ and } d_1 > 0 \\ & \text{or } \bar{\beta}_1 \leq \beta_{1,min} \text{ and } d_1 < 0 \\ 0 \text{ otherwise} \end{cases} \\ d_1 &= -\gamma_1 V_L i_L E_s/(C V_{max} V_{uc}) \end{aligned} \tag{11}$$

$$\begin{aligned} g_2 &= \begin{cases} -d_2 & \text{if } \bar{\beta}_2 \geq \beta_{2,max} \text{ and } d_2 > 0 \\ & \text{or } \bar{\beta}_2 \leq \beta_{2,min} \text{ and } d_2 < 0 \\ 0 \text{ otherwise} \end{cases} \\ d_2 &= \gamma_2 V_L i_L E_{fc}/V_{uc} \end{aligned} \tag{12}$$

$$\begin{aligned} g_{12} &= \begin{cases} -d_{12} & \text{if } \bar{\beta}_{12} \geq \beta_{12,max} \text{ and } d_{12} > 0 \\ & \text{or } \bar{\beta}_{12} \leq \beta_{12,min} \text{ and } d_{12} < 0 \\ 0 \text{ otherwise} \end{cases} \\ d_{12} &= -\gamma_{12} V_{fc} i_{fc} E_{fc}/V_{uc} \end{aligned} \tag{13}$$

where $\beta_{1,max}$, $\beta_{2,max}$, $\beta_{12,max}$ represent the upper bounds and $\beta_{1,min}$, $\beta_{2,min}$, $\beta_{12,min}$ represent the lower bounds of the parameters β_1, β_2, β_{12} respectively. We next study the stability property of the origin of $\epsilon = [E_s\ E_{fc}]^T$ with E_s and E_{fc} defined in Eqs.(5) and (6) respectively, under the control design and parameter adaptation laws proposed in Eqs.(5), (6), (10), (11), (12) and (13).

B. STABILITY ANALYSIS

We first present a discussion on the dynamics of the fuel supply system FSS, Fig.4. We assume that the specific dynamic equation of the FSS is unknown. It is however evident that the actual fuel flow $\dot{N}_f$ tracks the reference

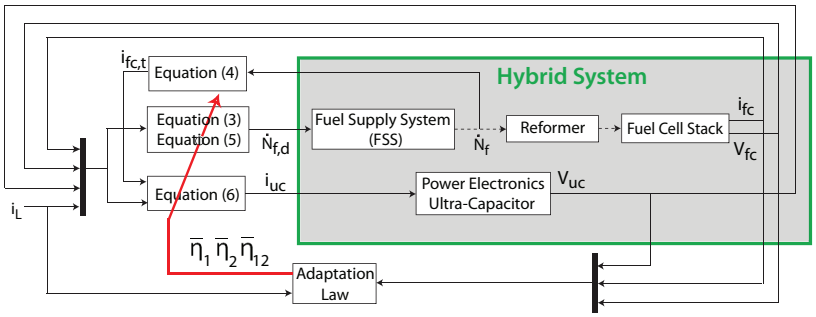

Fig. 4. Adaptive Control Approach

signal $\dot{N}_{f,d}$ with tracking error E_{fl}, where $E_{fl} = \dot{N}_f - \dot{N}_{f,d}$. Further, we assume that E_{fl} satisfies the condition

$$|E_{fl}| \leq \beta(|E_{fl}(0)|, t) + \gamma\left(\sup_{\tau \geq 0} |\dot{N}_{f,d}(\tau)|\right), \tag{14}$$

where β is a class $\mathcal{KL}$ function and γ is a class $\mathcal{K}$ function. The above equation essentially amounts to imposing that the tracking error is ultimately bounded by $\gamma\left(\sup_{\tau\geq 0}|\dot{N}_{f,d}(\tau)|\right)$, [23]. From Eq.(3), we have

$$\begin{gathered} \dot{N}_{f,d} = \sigma i_{fc,d},\ \dot{N}_f = \sigma i_{fc,t}, \\ \sigma = \mathcal{N}_{cell}\left[1-(1-U_{ss})\,k\right]/(4nFU_{ss}),\ \Rightarrow\ E_{fl} = \sigma E_{fc,t} \end{gathered} \tag{15}$$

where σ is constant. From Eqs.(14) and (15), we have

$$|E_{fc,t}| \leq \beta(|E_{fc,t}(0)|, t) + \gamma\left(\sup_{\tau \geq 0} |i_{fc,d}(\tau)|\right), \tag{16}$$

where $|E_{fc,t}|$ is ultimately bounded by $\gamma\left(\sup_{\tau\geq 0}|i_{fc,d}(\tau)|\right)$.

We choose the following Lyapunov function candidate

$$\bar{V} = \frac{1}{2}\left(\frac{\eta_2}{\eta_1}E_s^2 + k_d E_{fc}^2 + \frac{e_1^2}{\gamma_1} + \frac{e_2^2}{\gamma_2} + \frac{e_{12}^2}{\gamma_{12}}\right) \tag{17}$$

Differentiating $\bar{V}$ along the system trajectories produces Eq.(18). Note that η_1 and η_2 are not differentiated as they are treated as constant parameters.

$$\dot{\bar{V}} = \frac{\eta_2}{\eta_1}E_s\dot{E}_s + k_d E_{fc}\dot{E}_{fc} + \frac{e_1\dot{e}_1}{\gamma_1} + \frac{e_2\dot{e}_2}{\gamma_2} + \frac{e_{12}\dot{e}_{12}}{\gamma_{12}} \tag{18}$$

Using the equation of the ultra-capacitor dynamics and Eq.(5), where C is the capacitance,

$$\dot{V}_{uc} = \frac{-i_{uc}}{C}\ \Rightarrow\ \dot{E}_s = \frac{-i_{uc}}{CV_{max}}. \tag{19}$$

Manipulating Eq.(1) and combining it with Eq.(19) yields

$$\dot{E}_s = -\frac{V_L i_L - \eta_1 V_{fc} i_{fc}}{\eta_2 V_{uc} C V_{max}} \tag{20}$$

From the definition of E_{fc} in Eq.(6), the fuel cell current can be written as

$$\begin{gathered} E_{fc} = i_{fc} - i_{fc,t},\quad E_{fc,t} = i_{fc,t} - i_{fc,d} \\ i_{fc} = E_{fc} + E_{fc,t} + i_{fc,d} \end{gathered} \tag{21}$$

From Eqs.(5), (9), (20), (21) and (22) we have

$$\frac{\eta_2}{\eta_1}\dot{E}_s = \frac{V_{fc}(E_{fc}+E_{fc,t})}{CV_{max}V_{uc}} - \frac{V_L i_L e_1}{CV_{max}V_{uc}} - \frac{k_s E_s V_{fc}}{CV_{max}V_{uc}} \tag{22}$$

Also, from Eqs.(1), (6) and (9) we have

$$\begin{aligned} k_d\dot{E}_{fc} &= \left(V_L i_L e_2 - V_{fc} i_{fc} e_{12}\right)/V_{uc} - \alpha E_{fc} \\ \alpha &= k_p + \bar{\eta}_1 V_{fc}/(\bar{\eta}_2 V_{uc}) > 0 \end{aligned} \tag{23}$$

Equation (18) can be rewritten using Eqs.(9), (10), (11), (12), (13), (22) and (23), and noting that

$$\dot{e}_1 = -\dot{\bar{\beta}}_1,\ \dot{e}_2 = -\dot{\bar{\beta}}_2,\ \dot{e}_{12} = -\dot{\bar{\beta}}_{12}$$

as follows

$$\dot{\bar{V}} = -\epsilon^T Q \epsilon + \frac{V_{fc}E_s E_{fc,t}}{CV_{max}V_{uc}} - \frac{e_1 g_1}{\gamma_1} - \frac{e_2 g_2}{\gamma_2} - \frac{e_{12}g_{12}}{\gamma_{12}} \tag{24}$$

where,

$$Q = \begin{bmatrix} \frac{k_s V_{fc}}{CV_{max}V_{uc}} & \frac{-V_{fc}}{2CV_{max}V_{uc}} \\ \frac{-V_{fc}}{2CV_{max}V_{uc}} & \alpha \end{bmatrix},\quad \epsilon = [E_s\ E_{fc}]^T. \tag{25}$$

It should be noted that Q can be guaranteed to be positive definite by proper selection of the design parameters k_p and k_s. This is because C and V_{max} are constant and $V_{fc}, V_{uc} > 0$ are bounded based on the range of operating conditions. Further, note from Eqs.(9), (11), (12) and (13) that

$$e_1 g_1 \geq 0,\ e_2 g_2 \geq 0,\ e_{12} g_{12} \geq 0, \tag{26}$$

From Eqs.(24), (25), (26) and using the *Rayleigh Ritz Inequality* [24], we have

$$\begin{aligned} \dot{\bar{V}} &\leq -\epsilon^T Q\epsilon + \frac{V_{fc}}{CV_{max}V_{uc}}E_s E_{fc,t} \\ &\leq -\inf(\lambda_{min,Q})\|\epsilon\|^2 + \frac{V_{fc}}{CV_{max}V_{uc}}\|\epsilon\||E_{fc,t}| \\ &\leq -\inf(\lambda_{min,Q})(1-\theta)\|\epsilon\|^2 \\ &\quad +\|\epsilon\|\left(\frac{V_{fc}}{CV_{max}V_{uc}}|E_{fc,t}| - \theta\inf(\lambda_{min,Q})\|\epsilon\|\right) \\ &\leq -\inf(\lambda_{min,Q})(1-\theta)\|\epsilon\|^2, \quad \theta\in(0,1) \\ &\quad \forall\ \|\epsilon\| > \frac{V_{fc}}{CV_{max}V_{uc}\theta\inf(\lambda_{min,Q})}|E_{fc,t}| \end{aligned} \tag{27}$$

From Eq.(27), we have

$$\begin{aligned} \dot{\bar{V}} &\leq -\inf(\lambda_{min,Q})(1-\theta)\delta_{max}^2 < 0 \\ \forall &\quad \|\epsilon\| > \delta_{max} = \sup\left(\frac{V_{fc}}{CV_{max}V_{uc}\theta\inf(\lambda_{min,Q})}|E_{fc,t}|\right) \end{aligned} \tag{28}$$

From the boundedness property of $|E_{fc,t}|$ in Eq.(16) and from Eq.(5), we have

$$\delta_{max} = \sup\left(\frac{V_{fc}}{CV_{max}V_{uc}\theta\inf(\lambda_{min,Q})}\right)\gamma\left(\sup_{\tau\geq 0}|i_{fc,d}(\tau)|\right) \tag{29}$$

where,

$$\sup_{\tau\geq 0}|i_{fc,d}(\tau)| = \bar{\beta}_{1,max}\frac{V_L i_{L,max}}{V_{fc,min}} + k_s S_t. \tag{30}$$

Eqs.(29) and (30) show the existence of a δ_{max} for finite operating conditions. Next we show that state trajectories of the system converges to the region $\|\epsilon\| < \delta_{max}$ in finite time. Consider that at t_0, $\bar{V}(t_0)$ is finite and $\|\epsilon(t_0)\| > \delta_{max}$, and at time t, $\|\epsilon(t)\| = \delta_{max}$. Then, from Eq.(28) and applying the *Comparison Principle* [23], we have

$$\bar{V}(t) \leq \bar{V}(t_0) - (t-t_0)\inf(\lambda_{min,Q})(1-\theta)\delta^2_{max} \tag{31}$$

Noting from Eq.(17) that

$$\bar{V} \geq \frac{1}{2}min(\frac{\eta_2}{\eta_1}, k_d)\|\epsilon\|^2 \;\Rightarrow\; \bar{V}(t) \geq \frac{1}{2}min(\frac{\eta_2}{\eta_1}, k_d)\delta^2_{max},$$

we obtain

$$\Delta t = t - t_0 \leq \frac{\left[\bar{V}(t_0) - \frac{1}{2}min(\frac{\eta_2}{\eta_1}, k_d)\delta^2_{max}\right]}{\inf(\lambda_{min,Q})(1-\theta)\delta^2_{max}} \tag{32}$$

which represents a finite interval of time for finite initial conditions. In addition, by virtue of the design of parameter adaptation laws in Eqs.(10), (11), (12) and (13), the parameter estimates are bounded. Thus, the adaptive control design proposed in section III-A ensures that both $\|\epsilon\|$ and the parameter estimates remain bounded in the presence of an FSS that gives bounded tracking of demanded fuel $\dot{N}_{f,d}$.

C. OBSERVATIONS

We next make a few observations regarding the control design proposed above. Firstly, the adaptive control development leads to three parameters, namely β_1, β_2 and β_{12}, Eq.(7), although there are only two efficiencies involved. Correct estimation of these parameters is not guaranteed, and is not of utmost importance in this study. Secondly, from Eqs.(6) and (23), we can show through a Lyapunov analysis and through application of the *Barbalat's Lemma*, [23], that the proposed parameter adaptation laws in Eq.(10) causes $E_{fc} \to 0$. The proof is simple and is omitted for conciseness. This implies that the proposed control strategy guarantees $U = U_{ss}$ at steady-state.

Thirdly, we revisit the stability analysis, and consider an FSS with exponential tracking of the reference signal $\dot{N}_{f,d}$, which implies there exist constants $\gamma, \zeta, r_0 > 0$ such that

$$|E_{fl}(t)| \leq \gamma\,|E_{fl}(t_0)|\;e^{-\zeta(t-t_0)},\;\forall\;|E_{fl}(t_0)| < r_0 \tag{33}$$

From Eq.(15) we therefore have

$$|E_{fc,t}(t)| \leq \gamma\,|E_{fc,t}(t_0)|\;e^{-\zeta(t-t_0)},\;\forall\;|E_{fc,t}(t_0)| < r_0/\sigma \tag{34}$$

From Eq.(34) and *Converse Lyapunov Theorems* [23], there exists a positive definite $\bar{V}_{FSS}$ such that

$$\alpha_1 E^2_{fc,t} \leq \bar{V}_{FSS}(E_{fc,t}, t) \leq \alpha_2 E^2_{fc,t},\;\dot{\bar{V}}_{FSS} \leq -\alpha_3 E^2_{fc,t}, \tag{35}$$

where $\alpha_2 > \alpha_1 > 0$ and $\alpha_3 > 0$. Modifying the Lyapunov function of Eq.(17) to incorporate $\bar{V}_{FSS}$, we have

$$\bar{V} = \frac{1}{2}\left(\frac{\eta_2}{\eta_1}E_s^2 + k_d E_{fc}^2 + \frac{e_1^2}{\gamma_1} + \frac{e_2^2}{\gamma_2} + \frac{e_{12}^2}{\gamma_{12}}\right) + \bar{V}_{FSS} \tag{36}$$

Note from Eqs.(35) and (36) that $\bar{V}$ is positive definite and decrescent. Differentiating Eq.(36) along the system trajectories and proceeding as in section III-B, produces Eq.(37), where $\dot{\bar{V}}$ is negative semi-definite:

$$\dot{\bar{V}} \leq -\bar{\epsilon}^T\bar{Q}\bar{\epsilon},\;\text{where}\;\bar{\epsilon} = [E_s\;E_{fc}\;E_{fc,t}]^T, \tag{37}$$

$$\bar{Q} = \begin{bmatrix} k_s m & -\frac{m}{2} & -\frac{m}{2} \\ -\frac{m}{2} & \alpha & 0 \\ -\frac{m}{2} & 0 & \alpha_3 \end{bmatrix},\quad m = \frac{V_{fc}}{CV_{max}V_{uc}} > 0$$

where α is defined in Eq.(23). By proper choice of k_s and α, it can be ensured that $\bar{Q}$ is positive definite. For a bounded load, the voltages and currents of the fuel cell and ultra-capacitor will both remain bounded, as will their derivatives. Thus all of the error terms, and their derivatives, will also remain bounded. It is assumed that realistic load changes will occur through bounded derivatives. Thus, the conditions of Theorem 8.4 of [23] are satisfied and hence

$$\bar{\epsilon}^T\bar{Q}\bar{\epsilon} \to 0 \text{ as } t \to \infty \;\Rightarrow\; \bar{\epsilon} \to 0 \text{ as } t \to \infty$$

IV. EXPERIMENTAL RESULTS

We now present experimental results for the adaptive controller using a hardware-in-the-loop system developed in prior research, [14]. The system, shown in Fig. 5, implements the hybrid system schematically shown in Fig.2. The fuel cell

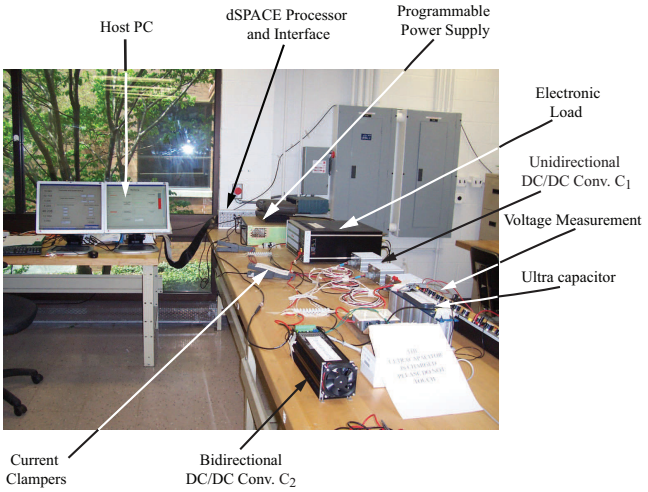

Fig. 5. Experimental Setup

model implements an SOFC system with 50 cells connected in series, each cell having an area of 251cm^2. For the system, $V_L = 24V$, $U_{ss} = 80\%$, and the target SOC $S_t = 0.8$. The ultra-capacitor has $C = 250$F and $V_{max} = 16.2$V. The

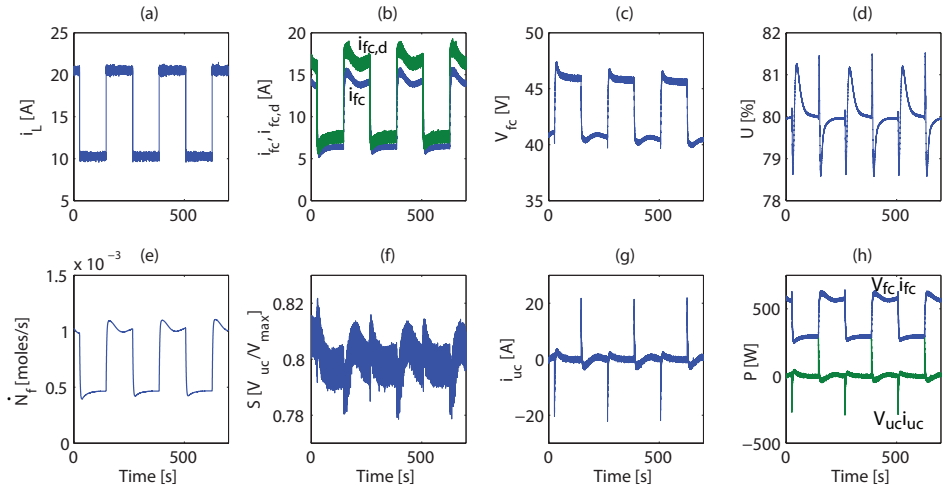

Fig. 6. Experimental Results

estimates of the efficiencies, $\bar{\eta}_1$ and $\bar{\eta}_2$, were each initialized at 0.92. Hence, $\bar{\beta}_1(0) = \bar{\beta}_2(0) = 1.087$ and $\bar{\beta}_{12}(0) = 1$. The FSS was modeled as $\dot{N}_f(s)/\dot{N}_{f,d}(s) = 0.85/(2s+1)$. This results in a 15% discrepancy between the delivered and the requested fuel flow at steady state. The above dynamical form is assumed unknown in the control design, and can be shown to yield the same structure of $|E_{fc,t}|$ as in Eq.(16).

The experimental results are shown in Fig.6. The controller parameters for this experiment were, $k_s = 70$, $k_p = 0.2$, $k_d = 4\text{x}10^{-5}$, $\gamma_1 = 40$, $\gamma_2 = 0.01$, and $\gamma_{12} = 0.01$. In the experiments, pulse loading was applied as shown in Fig.6(a). Fig.6(b) shows the fuel cell current demand $i_{fc,d}$ and current draw i_{fc}. Notice that i_{fc} is following $i_{fc,d}$ with an offset. This is due to the dynamics of the FSS as well as current regulation. The discrepancy between the fuel cell power and the load power is compensated by the ultra-capacitor, see Figs.6(g) and (h). Positive i_{uc} signify power draw and negative currents signify charging. Fig.6(g) demonstrates that the ultra-capacitor is used for transient power supply only while the fuel cell meets the bulk power demand. Figs.6(d) and (f) depict U and SOC S respectively. The controller was able to maintain each of these parameters within approximately 3% of their target value in spite of frequent and significant fluctuation in power demand.

In Fig.7, the parameter estimates are plotted. Figure 7(a), (b) and (c) depict the estimation of $\bar{\eta}_1$, $\bar{\eta}_2$, and $\bar{\beta}_{12}$ respectively. From Eq.(10) we note that for a bounded FSS, $\bar{\eta}_1$ can have a slope at steady state. This is confirmed in Fig.7(a). The slope changes sign every 120s when the load changes, but during the periods of constant load, the slope continues to increase (or decrease) as $E_s \nrightarrow 0$. If the load were not consistently pulsing, $\bar{\eta}_1$ would continuing growing (or diminishing) until it reached one of its imposed saturation limits, $\beta_{1,max}$ or $\beta_{1,min}$. Conversely, Figs.7(b) and (c) seem to show a converging tendency towards particular values between pulses. Since the slope of $\bar{\beta}_2$ and $\bar{\beta}_{12}$ are governed by E_{fc}, and $E_{fc} \to 0$ in steady-state, as discussed in section III-C, $\bar{\beta}_2$ (and hence $\bar{\eta}_2$) and $\bar{\beta}_{12}$ will tend to constant values in between pulses. It should be noted that these constant values are not guaranteed to be the true parameter values. The overall drift of $\bar{\eta}_2$ and $\bar{\beta}_{12}$ with time would continue until they reach one of their imposed saturation limits, $\beta_{2,max}$, $\beta_{2,min}$ or $\beta_{12,max}$, $\beta_{12,min}$.

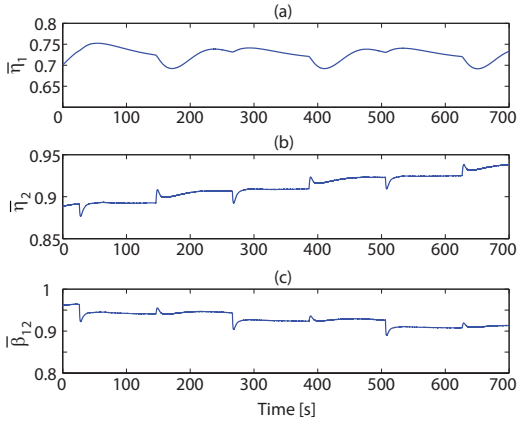

Fig. 7. Parameter Adaptation in Experimental System

Next we compare the control performances presented above with an FSS giving exponentially decaying tracking error. The later scenario was discussed in section III-C. For this scenario, the FSS was modeled as

$$\dot{E}_{fc,t} = -0.5E_{fc,t} \tag{38}$$

which has the same time-constant as used for the results in Figs.6 and 7. All other settings were kept identical as before for this test on the hardware-in-the-loop test-stand. As before the controller assumes no knowledge of the dynamic behavior of the FSS. Comparison results are presented in Fig.8. Figs.8(a1), (b1), (c1) and (d1) give results with bounded tracking and Figs.8(a2), (b2), (c2) and (d2) give results with exponential tracking. The control performance, as evident from the transient control of U and control of S, is very similar in both scenarios. However, the evolution of $i_{fc,d}$ and $\bar{\eta}_1$ are considerably different. The presence of tracking error causes $i_{fc,d}$ to be higher in the former case than the later, Figs.8(a1) and (a2). From Eq.(5) it is apparent that the higher $i_{fc,d}$ in the former case is primarily due to the lower $\bar{\eta}_1$ estimate than the later scenario, Figs.8(b1) and (b2). In fact, bounded tracking by FSS degraded the estimate of η_1, as specification documents of the uni-directional DC/DC

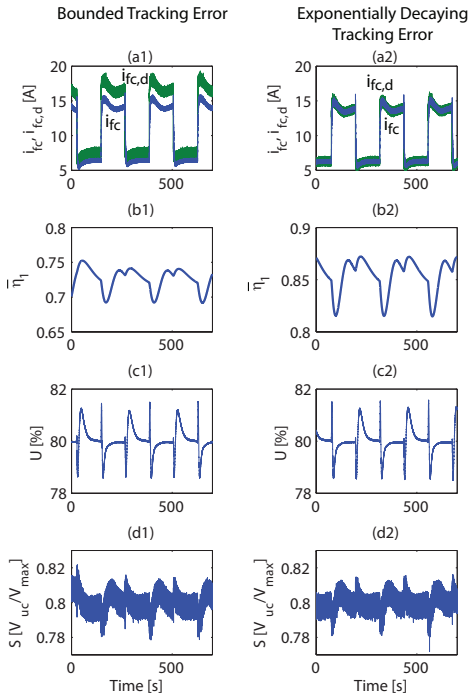

Fig. 8. Comparison of Control Performance under Bounded and Exponential Tracking Behavior of the FSS

converter indicates $80 - 88\%$ efficiency for the operating voltages of this test.

V. CONCLUSIONS AND FUTURE WORKS

In this paper, we design an adaptive controller for hybrid SOFC ultra-capacitor system. The controller incorporates a current regulation strategy for transient control of the fuel cell developed in prior research. Additionally, it maintains the state-of-charge of the ultra-capacitor at a desired level. The control design assumes the specific dynamic behavior of the fuel supply system (FSS) to be unknown, and considers a generalized FSS that gives bounded error in tracking the demanded fuel. For this generalized FSS, the controller ensures that state-of-charge of the ultra-capacitor is bounded around the desired level, in the presence of unknown DC/DC converter efficiencies, treated as parameters. The same design however admits asymptotic properties of the states, including the state-of-charge error, if the FSS displays exponentially decaying tracking error. Future work would include exploration of alternate and potentially more optimal means of expressing the generalized behavior of the FSS and investigating conditions that would yield convergence of the parameters to their true values.

REFERENCES

[1] J. Larminie and A. Dicks. *Fuel Cell Systems Explained*. John Wiley & Sons Ltd, Chichester, 2003.

[2] X. Li. *Principles of Fuel Cells*. Taylor and Francis Group, 2006.

[3] M. H. Nehrir and C. Wang. *Modeling and Control of Fuel Cells - Distributed Generation Applications*. John Wiley and Sons, Inc., 2009.

[4] J. R. Meacham, F. Jabbari, J. Brouwer, J. L. Mauzey, and G. S. Samuelsen. Analysis of stationary fuel cell dynamic ramping capabilities and ultra capacitor energy storage using high resolution demand data. *Journal of Power Sources*, 156(2):472 – 479, 2006.

[5] A. Drolia, P. Jose, and N. Mohan. An approach to connect ultracapacitor to fuel cell powered electric vehicle and emulating fuel cell electrical characteristics using switched mode converter. In *Industrial Electronics Society, 2003. IECON '03. The 29th Annual Conference of the IEEE*, volume 1, pages 897 – 901 vol.1, 2-6 2003.

[6] P. Thounthong, S. Ral, and B. Davat. Control strategy of fuel cell/supercapacitors hybrid power sources for electric vehicle. *Journal of Power Sources*, 158(1):806 – 814, 2006.

[7] A. Vahidi, A. Stefanopoulou, and H. Peng. Current management in a hybrid fuel cell power system: A model-predictive control approach. *Control Systems Technology, IEEE Transactions on*, 14(6):1047 –1057, nov. 2006.

[8] F. Mueller, J. Brouwer, F. Jabbari, and S. Samuelsen. Dynamic simulation of an integrated solid oxide fuel cell system including current-based fuel flow control. *Journal of Fuel Cell Science and Technology*, 3(2):144–154, 2006.

[9] W. Schmittinger and A. Vahidi. A review of the main parameters influencing long-term performance and durability of pem fuel cells. *Journal of Power Sources*, 180(1):1 – 14, 2008.

[10] A. Lazzaretto, A. Toffolo, and F. Zanon. Parameter setting for a tubular sofc simulation model. *Journal of Energy Resources Technology*, 126(1):40–46, 2004.

[11] K. Sedghisigarchi and A. Feliachi. Control of grid-connected fuel cell power plant for transient stability enhancement. In *Power Engineering Society Winter Meeting, 2002. IEEE*, volume 1, pages 383 – 388 vol.1, 2002.

[12] S. Campanari. Thermodynamic model and parametric analysis of a tubular sofc module. *Journal of Power Sources*, 92(1-2):26 – 34, 2001.

[13] T. Das and R. Weisman. A feedback based load shaping strategy for fuel utilization control in sofc systems. In *American Control Conference, 2009. ACC '09.*, pages 2767 –2772, 10-12 2009.

[14] T. Allag and T. Das. Robust nonlinear control of fuel cell ultracapacitor hybrid system. *American Control Conference, Baltimore MD*, 2010.

[15] Y. Guezennec, T. Choi, G. Paganelli, and G. Rizzoni. Supervisory control of fuel cell vehicles and its link to overall system efficiency and low-level control requirements. *Proceedings of the American Control Conference*, pages 2055–2061, 2003.

[16] J. Sun and I. Kolmanovsky. Load governor for fuel cell oxygen starvation protection: A robust nonlinear reference governor approach. *Proceeding of the 2004 American Control Conference, Boston, MA June 30 - July 2*, pages 828–833, 2004.

[17] A. Arce, A. J. del Real, and C. Bordons. Mpc for battery/fuel cell hybrid vehicles including fuel cell dynamics and battery performance improvement. *Journal of Process Control*, 19(8):1289 – 1304, 2009.

[18] P. Rodatz, G. Paganelli, A. Sciarretta, and L. Guzzella. Optimal power management of an experimental fuel cell/supercapacitor-powered hybrid vehicle. *Control Engineering Practice*, 13:4153, 2005.

[19] M. Uzunoglu and M. S. Alam. Dynamic modeling, design and simulation of a pem fuel cell/ultracapacitor hybrid system for vehicular applications. *Energy Conversion and Management*, 48:1544–1553, 2007.

[20] V. Paladini, T. Donateo, A. de Risi, and D. Laforgia. Super-capacitor fuel-cell hybrid electric vehicle optimization and control strategy development. *Energy Conversion and Management*, 48:3001–3008, 2007.

[21] Z. Jiang, L. Gao, and R. A. Dougal. Adaptive control strategy for active power sharing in hybrid fuel cell/ battery power sources. *IEEE Transactions on Energy Conversion*, 22(2):507–515, 2007.

[22] T. Das, S. Narayanan, and R. Mukherjee. Steady-state and transient analysis of a steam-reformer based solid oxide fuel cell system. *ASME Journal of Fuel Cell Science and Technology*, 7(1), 2010.

[23] H. K. Khalil. *Nonlinear Systems*. Prentice Hall, Upper Saddle River, NJ, third edition edition, 2002.

[24] W. J. Rugh. *Linear System Theory*. Prentice Hall, Upper Saddle River, NJ, 2 edition, 1996.